HYDROLOGICAL DEFORMATION OF KARST AQUIFERS DETECTED BY GPS MEASUREMENTS, MATESE MASSIF, ITALY

Authors: [1]Leone Guido*, [2]D'Agostino Nicola, [1]Esposito Libera, [1]Fiorillo Francesco

Affiliations: [1]Department of Sciences and Technologies, University of Sannio, Benevento, Italy; [2]Istituto Nazionale Geofisica e Vulcanologia, Rome, Italy

Corresponding author: Leone Guido*, email: *guleone@outlook.com*

Abstract

We used hydrological and geodetic observations to characterize the effects of hydrological forcing on the displacements observed by GPS (Global Positioning System) measurements collected by stations located in the karst area of the Matese massif (Apennines, central-southern Italy). The latter is one of the main karst massifs of the central-southern Apennines, characterized by steep slopes, high mountain peaks (up to 2050 m a.s.l.), and wide endorheic areas, playing a fundamental role in recharging the large groundwater resource of the massif. Integrated statistical analysis of rainfall and spring discharge time series provided insight into timescales characterizing the hydrological dynamic of the Matese massif, highlighting how hydraulic conditions of the water table at a specific time mainly depends on long antecedent periods of rainfall. Nevertheless, intense daily rainfall occurring during the wet season are responsible of the abrupt increase of the discharge of the Matese's springs, which show a typical karst behavior. Statistical analyses of time series show robust correlations between hydrological conditions of the karst aquifer and GPS displacements observed at stations placed over and around the massif. We find that the observed outward and inward deformations of the massif (horizontal dilatation and contraction) are controlled by water table variations, which are in turn controlled by temporal variations of the groundwater recharge due to rainfall. The detected patterns of deformation are intimately related to the seasonal and multi-year characteristics of the recharge/discharge processes, and allowed us to track with geodetic measurements the different phases of the water cycle in the karst aquifer of the Matese massif.

Key words: *Karst aquifer*, *deformation*, *GPS*, *spring discharge*, *Matese massif*

INTRODUCTION

The recent development of GNSS/GPS (Global Navigation Satellite System/Global Positioning System) networks (Blewitt et al. 2018) has shown that space-time redistribution of surface and groundwater masses determines a significant, measurable deformation of the Earth surface, providing an additional tool ("*hydrogeodesy*") for studying the water circulation (White et al. 2022). In the last years, GPS (Global Positioning System) continuous monitoring has shown that recharge/discharge phases of the karst aquifers hosted in the Mesozoic carbonates of central-southern Italy are strongly correlated with measured ground displacements (Silverii et al. 2016; Silverii et al. 2019), and modulate the continuous, long-term (~3-4 mm/yr) tectonic extension across the Apennines (D'Agostino 2014). Two main temporal patterns have been highlighted: a seasonal oscillation controlled by seasonal fluctuations of the aquifer hydrological stage, and a multi-year signal (long-term fluctuations) controlled by the occurrence of isolated or subsequent wet and dry periods (Silverii et al. 2016; Silverii et al. 2019; D'Agostino et al. 2018). In particular, an increase in frequency of meteorological dry (or drought) periods, along with an increase in mean annual temperature, have been observed in central-southern Apennine over the last thirty years, and appears the main cause of the decline of the groundwater storage observed for karst massifs of Mediterranean area (Fiorillo et al. 2021; Leone et al. 2021).

The strongest hydrological signal has been observed in horizontal components of displacements measured close to or inside karst aquifer areas, and has been associated to variations of the groundwater storage, though the deformation signal extended beyond the outcropping surface of the carbonate karst rocks (Silverii et al. 2019; Devoti et al. 2018).

As an example of these observations, **Figure 1** shows the horizontal daily displacements of a GPS station (*VAGA*) placed inside the area of the Matese karst massif (**Figure 2**), in southern Italy, together with daily discharge of a basal karst spring (Maretto spring, located 13 km from *VAGA*) draining the saturated zone of the karst aquifer and located along its southern side. The temporal correlation between hydrological data/trend and measured ground displacement is evident. In some cases, two displacement peaks can be observed in the wet season, both following peaks in the spring discharge. As the latter reflects the water table stage in the aquifer (Fiorillo 2011), the simplest explanation argues for a control of the hydraulic pressure in the aquifer saturated zone on the measured displacements.

The present study was built upon this observation and aims to describe the crustal deformation detected for the Matese karst massif, where several GPS stations are located inside the karst area, and others along its boundary. The observed phenomenon has been framed inside the local climate and hydrogeological context, and specific hydrological and statistical analyses were carried out to highlight the relationships between the different physical variables (rainfall, spring discharge, and ground displacement) and the respective time series.

1. STUDY AREA

The Matese massif is located in the median sector of the Apennine mountain range, and has an area of 540 km^2 (**Figure 2**). The morphology of Matese massif is characterized by steep slopes and surface elevations between 50 and 2050 m a.s.l. (the highest peak is the Miletto Mt.). More than 50% of the massif lies above 900 m a.s.l. and endorheic areas (**Figure 2**) occupies the most elevated zones (Leone et al. 2022). A highly permeable limestone and limestone-dolomite sequence of Triassic-Miocene age, with a thickness of 2500-3000 m, is exposed at the Matese massif. Faults have a prevalent NW-SE and NE-SW trends and dissect the sequence. The massif is tectonically juxtaposed by thrust faults to low permeability argillaceous complexes (Paleocene) and flysch sequences (Miocene) along the northern and eastern sectors (**Figure 2**). Normal faults bound the massif along the southern and western sectors and divide the massif from the Volturno alluvial Plain (Boncio et al. 2016, 2022; Galli et al. 2017). More specific insight into the geology of the area can be found in the Geological Map of Italy of Istituto Superiore per la Protezione e la Ricerca Ambientale (ISPRA; http://sgi.isprambiente.it/geologia100k/). The climate is Mediterranean: the maximum monthly precipitation occurs in November and the minimum in July, while the temperature and potential evapotranspiration patterns are almost opposite to that of precipitation, with the maximum occurring in July-August and the minimum in December-February. Because precipitation primarily occurs during the non-warm season, its distribution allows for the highest recharge into the aquifer (Fiorillo and Pagnozzi 2015). In the high-elevation zones (above 1000 m a.s.l.), precipitation is generally snowy during winter.

1.1. Hydrological karst features

The Matese massif represents a huge karst aquifer feeding numerous small springs as well as large basal springs. The basal karst springs are fed by the saturated zone of the aquifer, which is recharged by percolation thorough the vadose zone, locally characterized by a thickness up to hundreds or thousands of meters. Recharge occurs via both diffuse and concentrate way thanks to the presence of ponors and dolines located at the bottom of endorheic areas (Leone et al. 2022). The main spring groups are located along the southern side of the karst massif, inside the Piedimonte Matese and Telese Terme villages, and along the northern side, inside the Bojano village. These basal karst springs are thus located in the lowest ground zones, along the geological contact between karst and no-karst terrains.

The Torano spring (200 m a.s.l.) is located on the eastern cliff of a karst canyon and has a mean annual discharge of 2.0 m^3/s (Fiorillo et al. 2021), while the Maretto spring (170 m a.s.l.) is located at the foot of a limestone-dolomite slope in the Piedimonte Matese urban area, and has a mean annual discharge of 1.0 m^3/s (Fiorillo et al. 2021). Both the Torano and Maretto springs were tapped during the 1960s by the Campano aqueduct, which supplies the metropolitan area of Naples.

The Grassano-Telese springs (50-55 m a.s.l.) are placed along the southern side of Montepugliano relief, and are made by large fresh and sulfureous thermal springs closely located, with a mean annual discharge of 4.5 and 0.2 m^3/s, respectively (Fiorillo et al. 2019). Moreover, the Montepugliano relief is interested by a notable concentration of collapse sinkholes (22 sinkholes over an area of less than 1.5 km^2), connected to ascendant phenomenon of karst spring waters (Fiorillo et al. 2019) and the area surrounding this relief is the most important non-volcanic thermal area of Campania region (Rufino et al. 2021).

Along the northern side of the Matese massif, there are another three major groups of springs, having an overall mean annual discharge of 2.80 m^3/s (Civita 1969). These springs are fed by the karst system of the north-central sector of Matese massif and are located along debris deposits covering a fault separating limestone from flysch sequences (Petrella and Celico 2009). Most of the springs were tapped by Biferno Aqueduct during the 1960s and supply the Molise region. A branch of this aqueduct is joined with Campano Aqueduct through a tunnel in the eastern sector of Matese massif.

Many other karst springs are present on the Matese karst massif, and further details can be found in Fiorillo and Pagnozzi (2015).

As in many karst areas of the world, the surface hydrology of the Matese massif is characterized by numerous endorheic areas, which have been exploited during the last century to generate hydroelectric energy (Leone et al. 2022). The largest ones are connected to structural and tectonic features (faults, grabens), which control the form and dimension of the depressions, which are also known as poljes. Currently, some of them have seasonal lakes and are drained by one or more ponors. These endorheic areas have a fundamental role in the recharge processes of the karst aquifer, as rainfall cannot escape from the spring catchment through runoff. In particular, it has been estimated that only ≈30% of the rainfall, net of evapotranspiration, escape from the massif as runoff. The other amount (≈70%) recharges the aquifer (Fiorillo and Pagnozzi 2015). A detailed investigation of the Matese karst massif has allowed for mapping hundreds of these endorheic areas, most of them ($N = 271$) smaller than 0.33 km^2. In total, the endoreic areas occupy 167 of 540 km^2 of the entire karst massif (Leone at al. 2022). The largest endorheic area is that of Matese Lake polje (43.6 km^2), located between 1000 and 2050 m a.s.l. It is the major karst morpho-structural feature of the massif, whose evolution has been controlled mainly by WNW-ESE normal faults. The Matese Lake is a permanent water reservoir, sustained by fine sediments and pyroclastic ash coming from volcanos located along the Campania coast (Vesuvius and Phlegraean Fields), but it was modified by hydraulic works to avoid its water losses into ponors.

The endoreic areas of the Letino and Gallo Lakes are effectively dam reservoirs. The lakes were created by the interruption of the Lete and Sava Rivers, respectively, but can be considered part of wide endoreic areas. In fact, before dam construction, both rivers sunk into two ponors located downstream the dams.

The Campitello endorheic area is another important karst feature of the Matese massif. The area gets flooded during rapid snow melting periods and a temporary lake forms. A ponor located at 1417 m a.s.l. in the central part of the Campitello plain drains the lake water, which dries out in several days.

2. DATA AND METHODS

Table 1 shows information about stations and the relative daily time series used in this study, which are illustrated in **Figure 3**. The various hydrological and geodetic observations extend over a period of about 15 years, with different data coverages.

Daily rainfall and temperature data have been provided by Multi-risk Functional Center of Civil Protection of Campania Region (http://centrofunzionale.regione.campania.it/#/pages/dashboard). Even if there are several rain gauges surrounding the Matese massif, analyses were primarily carried out using the daily measurements of the Alife rain gauge and thermometer (*S1*, 117 m a.s.l.), because of its continuous records, without interferences connected with snowy precipitation. Rainfall time series was used to define the input hydrological signal controlling spring discharge and, consequently, the ground displacements recorded at GPS sites. Instead, the Letino rain gauge (*S2*, 1050 m a.s.l.) was used in simulation of the karst aquifer recharge, given its suitable elevation.

Discharges of Torano and Maretto springs were provided by the Aqueduct company managed by the Regione Campania. These discharge data were used because of the continuity of the records and quality of the measurements at daily scale.

Stations from various GNSS/GPS networks were considered, which provided continuous raw displacement data. In particular, the *VAGA*, *LNGN* and *PTRJ* stations belong to the INGV RING GNSS/GPS network (http://ring.gm.ingv.it), the *VINC* station belongs to the NETGEO GNSS/GPS network (http://www.netgeo.it), and the *ALIF* station to the Campania Regional GNSS/GPS network (http://gps.sit.regione.campania.it/indexmain.php). GPS data are reduced using the Jet Propulsion Laboratory (JPL) GIPSY-OASIS II software (ver. 6.3) in a Precise Point Positioning (Bertiger et al. 2010) mode, updating the results of D'Agostino et al. (2018), where the full processing is described in detail. Since the primary focus of this work is the deformation of hydrological origin, we removed the secular, tectonic, linear trends (see D'Agostino 2014 for their tectonic implications), estimated with a weighted least-squares approach. When seasonal signals are taken into account, typical daily scatter of daily position time series are ~1 mm and ~4 mm for horizontal and vertical components, respectively (Blewitt et al. 2018).

Time series were managed and analyzed by MATLAB (ver. 2019b) software. In particular, cross-correlation analysis was carried out to evaluate statistical correlations between rainfall and spring discharge, and between hydrological variables and GPS-measured displacements. Fast Fourier Transform-based (FFT-based) analysis and Gaussian-weighted moving average (Gaussian smoothing) were successively used to highlight the seasonal and multi-year fluctuations in time series.

Table 1 Hydrological and GPS time series used in the study. The elevation (in m a.s.l.), latitude and longitude (in decimal degree), and length of the available time series are summarized for each station and karst spring.

			Location			Time interval of daily data
			Elevation	Latitude	Longitude	
GPS station	*Within karst massif*	VAGA (*Valle Agricola*)	736	41.415	14.234	15 Mar 2005-31 Oct 2020
		LNGN (*Longano*)	1021	41.501	14.253	2 Jun 2006-3 Dec 2016
		PTRJ (*Pietraroja*)	1065	41.364	14.529	19 Jul 2006-31 Oct 2020
	Outside karst massif	ALIF (*Alife*)	109	41.327	14.335	25 Sep 2008-31 Oct 2020
		VINC (*Vinchiaturo*)	514	41.468	14.562	28 Jan 2012-31 Oct 2020
Rain gauge and thermometer		S1 (*Alife*)	117	41.339	14.334	15 Mar 2005-31 Oct 2020
		S2 (*Letino*)	1050	41.454	14.253	31 Oct 2008-31 Oct 2020
Karst spring		Maretto	170	41.358	14.370	15 Mar 2005-31 Oct 2020
		Torano	200	41.365	14.381	15 Mar 2005-31 Oct 2020

2.1. Cross-correlation analysis and rainfall data pre-processing

The cross-correlation function describes the similarity, or correlation, between a time series x and the lagged versions of another time series y as a function of the time lag (k-lag). The similarity between time series is expressed by the Pearson correlation coefficient, $r_{xy}(k)$, which varies between −1 (maximum negative correlation) and +1 (maximum positive correlation).

In particular, the linear cross-correlation function, $r_{xy}(k)$, is defined as (Larocque et al. 1998):

$$r_{xy}(k) = \frac{C_{xy}(k)}{\sigma_x \sigma_y}$$

where $C_{xy}(k)$ is the covariance between the time series of x and y variables computed at time lag k, while σ_x and σ_y are the standard deviations of the time series. Typically, when analyzing the link between the climate and a specific groundwater variable (spring discharge, or water level), time series of the independent variable x is the time series of rainfall, while the lagged time series of y is represented by spring discharge. Instead, when evaluating the correlation between hydrological and GPS observations, x represents rainfall or spring discharge and y is the displacement.

In our investigation, cross-correlation analysis was used to evaluate statistical similarities between time series of the different variables and the time scale characterizing the processes under investigation.

First, it must be remarked that daily rainfall cannot completely explain measured spring discharge value at specific time, which rather depends on the long antecedent period of rainfall (Fiorillo and Doglioni 2010). Therefore, cross-correlation analysis was primarily used to estimate the period of antecedent rainfall explaining the observed spring discharge. This analysis involved the pre-processing of the daily rainfall data, to construct multiple continuous time series of the cumulative rainfall. These time series were obtained by summing daily values in a time window of fixed width, which has then been moved one step forward through the whole time series. In this study, window width varies from 1 to 360 days.

2.2. Detection of seasonal and multi-year fluctuations of hydrological and GPS time series

A hydrological time series is a sequence of measurements of a specific hydrological variable in chronological order. Measured values of hydrological variables, such as daily rainfall, spring discharge, and air temperature, show temporal variations due to different physical processes which, in turn, continuously evolve over time.

Variations observed in hydrological time series are ascribable to five components, which are the long-term trend in mean (and/or variance), seasonality, cyclicity, jumps and randomness (Beaumont 1982; Caswell 1991). In the hypothesis that hydrological processes affect the motion of the land surface, and thus displacement measurements, the hydrological patterns observable in hydrological time series would be recorded by GPS stations and recognizable in the displacement recorded over the time.

In practice, GPS measurements are affected by a number of factors and include random and systematic noises from different sources, which could make the hydrologically induced displacement difficult to recognize and quantify (Blewitt 2015). To this scope, the Fast Fourier Transform-based (FFT-based) analysis and Gaussian-weighted moving average (Gaussian smoothing) were used in this study, allowing us to emphasize the short- and long-term oscillations in the time series. The time patterns characterizing the hydrological series was then compared to those identified in GPS time series to highlight any similarities among the two kinds of signals.

In particular, the Gaussian smoothing, was used to outline trend component of time series, that is, the long-term variations in spring discharge, rainfall and ground motion. The Gaussian smoothing belongs to moving average smoothing methods (Fei and Jin 2016), which are classical approaches used in estimating time series trend (Caswell 1991; Hyndman and Athanasopoul 2018). Gaussian smoothing was preferred to classical moving average method in this study because it is more effective in reducing the short-term fluctuations. A 4-year time window was used for Gaussian smoothing, to eliminate the effect of short-term fluctuation due to hydrological seasonality.

On the other hand, the FFT-based filtering was applied to emphasize the short-term cyclic (seasonal) oscillations of time series superimposed on the trend component. In this case, this method was preferred instead of Gaussian filtering as it provided more suitable results for time series characterized by significant data gaps and data dispersion. More precisely, the FFT-based analysis was applied to decompose time series into a series of sinusoids of varying amplitude, phase, and frequency (Kramer 1996; Fleming et al. 2002; Box et al. 2016). The main components making a significant contribution to the time series were selected by analyzing the Fourier amplitude spectra, which describe how the amplitudes of a signal are distributed among different frequencies (Kramer 1996). Finally, smoothed time series were reconstructed by summing together the few components having the highest amplitudes.

3. RESULTS

Time series analyses carried out in this study aimed to ascertain the link between hydrological processes and ground displacement detected through continuous GPS measurements in the area of the Matese karst massif.

3.1. Relationships between rainfall and karst spring discharge

Daily rainfall does not fully explain the spring discharge at specific time. On the other hand, rainfall cumulated over long time periods can describe the dynamic of the karst springs and, thus, of the karst aquifer (Fiorillo and Doglioni 2010). Based on this consideration, cross-correlation analysis was performed between daily rainfall and spring discharge time series to evaluate the period of cumulate rainfall which better explains the groundwater dynamic of the Matese karst massif.

Table 2 and **Figure 4** show the results of cross-correlation analysis between rainfall cumulated over different periods (from 1 to 360 days) and daily spring discharge. It can be seen how the Pearson correlation coefficient $r_{xy}(k)$ increases with increasing k-lag (in days) for short rainfall periods, while it is maximum when reducing k-lag and increasing the period of cumulative rainfall beyond three months. This indicates that the spring discharge is mainly controlled by rainfall cumulated over long-time periods, at least up to 270 days. As shown by **Table 2**, the highest correlation coefficient and the lowest k-lag were obtained for rainfall cumulated over periods of 180 and 270 days.

Table 2 Results of the cross-correlation analysis between daily time series of rainfall cumulated over period of different length (periods from 1 day up to 360 days) and discharge of Torano and Maretto karst springs. The maximum value of the Pearson correlation coefficient, $r_{xy}(k)$, and the relative k-lag (in days) are shown in table.

Period of cumulate rainfall	Torano spring		Maretto spring	
	$r_{xy}(k)$	k-lag	$r_{xy}(k)$	k-lag
1 day	0.121	97	0.141	93
7 days	0.245	92	0.287	92
15 days	0.318	88	0.375	91
30 days	0.408	85	0.485	90
60 days	0.511	60	0.610	78
90 days	0.600	47	0.686	51
120 days	0.644	27	0.729	43
180 days	0.742	1	0.776	10
270 days	0.689	0	0.705	0
360 days	0.597	0	0.489	0

3.2. Relationships between hydrological variables and ground displacement

The results of the analysis described in the previous section highlighted the overall timescales characterizing the hydrological dynamic of the Matese massif, where spring discharge at a specific time primarily depends on the rainfall which has occured during the antecedent 180-270 days.

Starting from this result, a further cross-correlation analysis was carried out between hydrological records (180- and 270-day rainfall and spring discharge) and raw GPS displacement data. Results of the analysis are summarized in **Figure 5** and **Table 3**, and provided insight into the correlation between hydrological processes and ground displacement, and the average response time of the ground motion to variations of the aquifer hydrological stage.

We observe that the displacements in the horizontal plain are linearly (positively or negatively) correlated with hydrological stages of the aquifer. Conversely, if excluding the *LNGN* GPS stations, the vertical displacement at single sites would not show any clear correlation with the hydrological variables ($|r_{xy}(k)| < 0.3$).

Horizontal displacements recorded at *VAGA* GPS station (**Figure 5a**) are strongly, negatively correlated with 6-month rainfall and spring discharge. This indicate that the station moves south-westward, i.e., outward from the massif, toward the alluvial plain of the Volturno River, during high groundwater stages. The time lag between the hydrological forcing and displacement varies from few days up to 21 days, and it is lower for the east component than for the north component.

Displacements of the *ALIF* station (**Figure 5b**) appear consistent with those of the *VAGA* station. In fact, displacement in the north direction is negatively correlated with Torano spring discharge and 6-month cumulative rainfall, while there would be no clear correlation of the hydrological variables with the east and vertical components of the displacement.

For the *LNGN* GPS station (**Figure 5c**), the hydrological stages mainly affect displacements in the north direction. The north component is strongly, positively correlated with rainfall and spring discharge, highlighting that the station moves toward north during aquifer recharge and hydrological wet periods. The coefficient $r_{xy}(k)$ is maximum for k-lags between 0 and 6 days. On the contrary, a time lag of 134 days characterizes the cross-correlation function associated with the east component, which appears weakly, negatively correlated with hydrological variables.

The east component of displacement of *PTRJ* GPS station (**Figure 5e**) is characterized by quite high, positive values of the cross-correlation coefficient. Differently from the *VAGA* and *LNGN* stations, the *PTRJ* station move toward east

during high hydrological stages. This hydrologically induced displacement appears lagged of 90 days with respect to spring discharge and 31 days with respect to 9-month cumulative rainfall. No correlation would appear for the north component with hydrological variables.

Data records of the *VINC* GPS station (**Figure 5d**) also appears in line with those of the stations placed on the karst massif. Horizontal displacements in the north and east directions are positively correlated with spring discharge and 6-month rainfall. Thus, the station would move toward both east and north during hydrologically wet periods and toward south and west during dry periods. Displacements are lagged with respect to the hydrological forcing and time lags are significatively shorter for the east component than for the north component.

Table 3 Results of the cross-correlation analysis between hydrological time series and GPS time series. Statistically significant values of the Pearson correlation coefficient, $r_{xy}(k)$, and the relative k-lag (in days) are shown in table. The 9-month cumulative rainfall was considered for the *PTRJ* GPS station and the 6-month cumulative rainfall for the other stations.

GPS station	Displacement component	Cumulative rainfall		Torano spring		Maretto spring	
		$r_{xy}(k)$	k-lag	$r_{xy}(k)$	k-lag	$r_{xy}(k)$	k-lag
VAGA	*Nord*	-0.887	21	**-0.838**	17	**-0.878**	10
	East	-0.872	13	**-0.814**	10	**-0.852**	3
	Vertical	-	-	-	-	-	-
ALIF	*Nord*	-0.484	96	**-0.510**	74	-0.437	68
	East	-	-	-	-	-	-
	Vertical	-	-	-	-	-	-
PTRJ	*Nord*	-	-	-	-	-	-
	East	0.533	31	0.472	88	0.372	89
	Vertical	-	-	-	-	-	-
VINC	*Nord*	0.412	101	0.407	98	0.449	82
	East	0.452	41	0.459	9	0.317	9
	Vertical	-	-	-	-	-	-
LNGN	*Nord*	0.732	6	**0.731**	2	**0.706**	0
	East	-	-	-0.368	133	-0.359	130
	Vertical	0.388	0	0.348	0	0.357	0

In summary we observe a strong correlation between the horizontal displacements and the hydrological phases of recharge/discharge of the Matese massif. The time lags of cross-correlation values $|r_{xy}(k)| > 0.5$ between spring discharge and GPS displacements yield an average value of 16 days suggesting a very fast deformational response to the hydrological forcing. Conversely, the low values of cross-correlation coefficient associated with the vertical displacements imply their negligeable contribution to the accommodation of the hydrological forcing.

3.3. Hydrological patterns in time series of the ground displacement

FFT-based and Gaussian filtering were carried out to emphasize short- and long-term oscillations in time series with the aim of ascertain any recognizable hydrological patterns in GPS measurements of the ground motion.

Figure 3 compares time series of hydrological and GPS data. In particular, for each panel in Figure 3, the raw measurements, the long-term mean of the time series (□; black dashed line), the filtered time series computed from FFT-based analysis (continuous solid line), and the Gaussian smoothing (red dashed line) are plotted.

It should be noted that the mean displacement values in **Figure 3e-n**, D_{north} = 0 mm and D_{east} = 0 mm, represent the intersection of the north and east axes. Thus, positive displacement values indicate that a specific GPS station moves to the north and east quarters, while negative values indicate that the station moves towards the south and west quarters.

Figures 3a, **b** and **d** confirm results of cross-correlation analysis, as both short- and long-term variations of the rainfall cumulated over a period of 180 days (R_{180}, **Figure 3d**) closely follow spring discharge fluctuations (**Figure 3a**, **b**), highlighting that the hydrological stage of the massif at any time strongly depends on the previous period of rainfall. The range between □ –□σ and □ + σ has been drawn in **Figure 3d**, which represents the normal rainfall condition in the reference period (□ and σ are the long-term mean and standard deviation of the time series, respectively). Drought years characterized by below-normal rainfall amounts can be observed in 2007, 2012, 2017. Drought years mark the end of decreasing rainfall periods, which are the main cause of groundwater storage drying and, thus, of spring discharge decline (**Figure 3a**, **b**). The recovery of the spring discharge following meteorological droughts is related to significant increases of the rainfall amounts, which are marked by peaks in the rainfall time series higher than □ + σ.

A seasonal component is present in time series of the ground displacement. In addition, the hydrological patter characterizing spring discharge and rainfall is well recognizable in the GPS time series of the horizontal displacement (**Figure 5e-n**), indicating that the karst massif responds to seasonal and long-term variations of the groundwater storage, as well as to abnormal increases or decreases of the recharge. Sequences of consecutive dry (or wet) years can be observed in **Figure 3d**, which give rise to periods of below average (or above average) groundwater storage and spring discharge. Such a low-frequency hydrological variation (red dashed line in **Figure 3**) affects the ground displacement and is clear in the long-time series of the *VAGA* GPS station (**Figure 3e**, **f**) and *PTRJ* (**Figure 3j**), and in shorter time series of *VINC* (**Figure 3l**), and *LNGN* (**Figure 3m**) stations as well. Furthermore, a strong hydrological signal is associated with droughts, such as those of 2007, 2012 and 2017, which are marked by low downward peaks in GPS time series.

Although a seasonal component was detected also in time series of the vertical displacement, the hydrological patterns are not clearly evident in this case. As already discussed by Silverii et al. (2019), a low signal-to-noise ratio generally characterizes time series of the vertical displacement of an individual GPS station, which could obscure the hydrological patterns, and data from several stations are required to enhance the signal-to-noise ratio.

3.4. Strain analysis

To investigate the overall deformation response of the Matese karst massif to hydrological forcing we calculated the temporal variation of the strain tensor in the area defined by the polygon obtained by joining the five GPS stations (**Figure 6** and Supplementary Material). The spatial derivatives of the stations displacements u in the x (North) and y (East) directions define the components of the displacement gradient tensor:

$$\frac{\partial u_x}{\partial x}, \frac{\partial u_x}{\partial y}, \frac{\partial u_y}{\partial x}, \frac{\partial u_y}{\partial y}$$

The displacement gradients (extension positive) are then used to calculate the components of the symmetric strain tensor:

$$\varepsilon_{xx} = \frac{\partial u_x}{\partial x}, \qquad \varepsilon_{yy} = \frac{\partial u_y}{\partial y}, \qquad \varepsilon_{xy} = \varepsilon_{yx} = \frac{1}{2}\left[\frac{\partial u_x}{\partial y} + \frac{\partial u_y}{\partial x}\right]$$

The principal axes of the strain tensor are then calculated as:

$$\varepsilon_1, \varepsilon_2 = \frac{\epsilon_{xx} + \varepsilon_{yy}}{2} \pm \sqrt{\left(\frac{\epsilon_{xx} - \varepsilon_{yy}}{2}\right)^2 + \varepsilon_{xy}^2}$$

where ε_1, ε_2 are the magnitudes of the most extensional (extension positive) and compressional eigenvalues of the strain rate tensor. The direction θ of the most extensional eigenvalue (counter-clockwise from East) is finally given by the following relationship:

$$\tan(2\theta) = \frac{2\varepsilon_{xy}}{\varepsilon_{xx} - \varepsilon_{yy}}.$$

To emphasize the seasonal and multi-year response we used the horizontal components of the FFT-filtered time series (**Figure 3**) of five stations in and around the Matese massif, resampled at time steps of 0.01 years. For each epoch in the time interval of simultaneous activity of the five stations (January 2012-December 2016), we estimated with a weighted least-squares approach the components of the displacement gradients and the strain tensor. **Figure 6** illustrates two snapshots of the continuous strain tensor, representative of dry (low water table, November 2012) and wet (high water table, May 2013) conditions (the complete continuous evolution is available as an animation in Supplementary Material). The inset in **Figure 6** shows the evolution of the dilatational strain ($\varepsilon_{xx} + \varepsilon_{yy}$) compared to the discharge of the Torano and Maretto springs. A low water table condition (November 2012) corresponds to inward displacements and negative (contractional) dilatational strain up to -4×10^{-7} relative to the average of the 2012-2017 period. A high water table condition (May 2013) corresponds to outward displacements of the stations in the Matese massif and positive (extensional) dilatational strain. The maximum amplitude of the average hydrological strain across the Matese massif is approximately 6×10^{-7} and is probably not homogeneously distributed, although the lack of a dense station coverage halts a more accurate analysis.

4. DISCUSSION AND CONCLUSION

This study deals with the link between karst aquifer hydrological stage and crustal deformation, detected for the Matese massif. Time series of hydrological data were used to represent the hydrological stage of the karst system, which is the hydraulic condition of the karst aquifer at a certain time. In turn, the hydraulic conditions depend on water table level in the saturated zone, that is the groundwater storage, as well as the water level in shafts connected to the saturated zone. Shaft has a crucial role in groundwater dynamics since they drain water rapidly, causing a fast recharge into the saturated zone and, eventually, the raising of the water table level (Fiorillo 2011). The abrupt increases of the discharge observed in spring hydrographs following intense rainfall events are also generally associated with the rise of the water level in conduits above the saturated zone (Bonacci and Zivaljevic 1993; Bonacci 1995; Drogue 1980; Ford and Williams 2007). Direct measurements of the water level into karst aquifer are unavailable for the Matese massif, and records of daily discharge of Torano and Maretto springs were considered as a proxy for the water table fluctuations. To investigate more in detail the relationship between spring discharge and GPS measured displacement, we simulated the recharge process during the 2009-2010 hydrological year (**Figure 7**), using the recharge model developed by Fiorillo et al. (2015a) and calibrated by Fiorillo and Pagnozzi (2015). This model transforms the daily rainfall into excess rainfall, P_{exc}, through the hydrological balance of the soil (**Figure 7b**). The P_{exc} is the amount of rainfall which is free to infiltrate in depth into the vadose zone (recharge) or to run off when a specific threshold (24.3 mm) is exceeded. This threshold value has been calibrated from long term annual hydrological balance of karst massif (Fiorillo et. al. 2015a; Fiorillo and Pagnozzi 2015). The runoff allows the surficial water to leave the karst massif without any contribute to recharge process. In the endorheic areas, however, surficial water can be considered as "internal runoff" (White 2002), that totally contributes to recharge by concentrate infiltration into ponors and dolines or leakage from bottom of endorheic areas. According to our model

rainfall is retained as soil moisture into the soil mantle up to the field capacity until the end of November or it is lost through evapotranspiration processes (**Figure 7b**). During this period, the hydrograph highlights the recession of the spring (**Figure 7c**). The rainfall of early December causes the beginning of the recharge processes and interrupts the spring discharge recession. Snowy precipitations occurring during winter postpone the infiltration processes. Looking at **Figure 6c**, GPS displacements also invert the trend in December. Successively, the intense rainfall of early January generates the diffuse and concentrate recharge, which in turn causes the rapid increase of the spring discharge, and the acceleration of the GPS station as well (**Figure 7c**). Up to mid-March, recharge processes sustain high flow rate, then discharge decreases due to decrease of rainfall. The GPS site experiences the maximum displacement in this period, which seems shifted forward of about 1 month with respect to the peak of the spring discharge. The end of recharge processes starts from early June, and soil moisture begins to accumulate a water deficit. Spring discharge decreases since April, and it can be considered no longer affected by recharge processes from June. GPS displacement also decreases in the same period.

Our observations indicate a close relationship between hydrological conditions in the karst aquifer and the observed deformation of the Matese massif. **Figure 8** shows two different stages of the water table (low- and high-stand), corresponding to a low and high spring discharge condition in **Figure 6**, and the connected deformation observed at the GPS stations.

Similar to other areas in the central and southern Apennines (Silverii et al. 2016; Silverii et al. 2019), the hydrological forcing dominantly affects the horizontal deformations, with minor impact on vertical displacements. As observed by Silverii et al. (2016) for the Irpinia region, the vertical component displays seasonal and multiyear signals more homogeneously distributed in space, independently from extent of the karst aquifers and closely correlated with regional estimates of total water storage. The different sensitivity of the horizontal components to the hydrologically induced deformation processes, allow us to temporally resolve the maximum hydraulic head in the karst aquifer. We suggest that the main mechanism controlling the observed horizontal transient signal is the effect of time-dependent water pressure which induces the rock mass strain, void and fluid-filled volume change, as consequence of the poroelastic behavior of the karst aquifer. Conductive water-filled fracture systems could have an important role in controlling the anisotropic deformation along the different directions. However, the extent at depth of this process is unclear. In other part of the Apennines (D'Agostino et al. 2018) hydrological seasonal modulation appear to control the nucleation of low-magnitude seismicity in the shallow suggesting that the effect of hydrological forcing extend to the first kilometers (0-6 km) of the crust.

Finally, we remark that the observed pattern of hydrologically-related deformation is intimately connected to the specific pattern of recharge of the karst aquifers in the Apennines (Fiorillo et al. 2015b). Slow groundwater circulation and multiyear variations of the water table elevation, allows significant variations of the stored groundwater, that, in turn, control the observed pattern of deformation.

Supplementary Material (SI)

Movie 1. Animation of horizontal GPS displacements at stations in the Matese massifs (red vectors) and the associated evolution of the principal axes of the strain tensor (diverging/converging green vectors) in the polygon joining GPS stations (black line). Areas with outcropping carbonate rocks are emphasized with a blueish tone. The diagram in the upper right shows the temporal evolution of the horizontal dilatational strain ($\varepsilon_{xx} + \varepsilon_{yy}$) and the discharge at Torano-Maretto springs highlighting the strong correlation between horizontal deformation and hydraulic conditions in the Matese aquifer.

REFERENCES

Beaumont C (1982) The analysis of hydrological time series. Progress in Physical Geography: Earth and Environment 6(1):60–99. https://doi.org/10.1177/030913338200600103

Bertiger W, Desai S, Haines B, Harvey N, Moore A, Owen S, Weiss J (2010) Single receiver phase ambiguity resolution with GPS data. J Geod 84(5):327–337. https://doi.org/10.1007/s00190-010-0371-9

Blewitt G (2015) GPS and space-based geodetic methods. In: Schubert G (ed) Treatise in Geophysics, 2nd edn. Elsevier, Oxford, pp 307-338. doi:10.1016/B978-0-444-53802-4.00060-9.

Blewitt G, Hammond WC, Kreemer C (2018) Harnessing the GPS Data Explosion for Interdisciplinary Science. Eos 99:12. https://doi.org/10.1029/2018EO104623

Bonacci O, Zivaljevic R (1993) Hydrological explanation of the flow in karst: example of the Crnojevica spring. J Hydrol 146:405–419

Bonacci O (1995) Ground water behavior in karst: example of the Ombla Spring (Croatia). J Hydrol 165:113–134

Boncio P, Dichiarante AM, Auciello E, Saroli M, Stoppa F (2016) Normal faulting along the western side of the Matese Mountains: Implications for active tectonics in the Central Apennines (Italy). J Struct Geol 82:16–36. https://doi.org/10.1016/j.jsg.2015.10.005.

Boncio P, Auciello E, Amato V. Aucelli P, Petrosino P, Tangari AC, Jicha BR (2022) Late Quaternary faulting in the southern Matese (Italy): implications for earthquake potential and slip rate variability in the southern Apennines. Solid Earth 13:553–582. https://doi.org/10.5194/se-13-553-2022.

Box GE, Jenkins GM, Reinsel GC, Ljung GM (2016) Time series Analysis. Forecasting and Control. John Wiley & Sons, Hoboken, New Jersey.

Caswell F (1991) Success in Statistics. John Murray Educ., England.

Civita M (1969) Valutazione analitica delle riserve in acque sotterranee alimentanti alcune tra le principali sorgenti del massiccio del Matese (Italia meridionale), in Italian. Mem Soc Nat Napoli 78:133–163.

D'Agostino N (2014). Complete seismic release of tectonic strain and earthquake recurrence in the Apennines (Italy). Geophys Res Lett 41:1155–1162. https://doi.org/10.1002/2014GL059230

D'Agostino N, Silverii F, Amoroso O. Convertito V, Fiorillo F, Ventafridda G, Zollo A (2018) Crustal Deformation and Seismicity Modulated by Groundwater Recharge of Karst Aquifers. Geophys Res Lett 45(22):253–262. doi:10.1029/2018GL079794

Devoti R, Riguzzi F, Cinti FR, Ventura G (2018) Long-term strain oscillations related to the hydrological interaction between aquifers in intra-mountain basins: A case study from Apennines chain (Italy). Earth & Planet Sci Lett 501:1–12. https://doi.org/10.1016/j.epsl.2018.08.014

Drogue C (1980) Essai d'identification d'un type de structure de magasins carbonatés fissurés: application à l'interprétation de certains aspects du fonctionnement hydrogéologique. Mémoire hors série de la Société Géologique de France 11:101–108

Fei Z, Jin F (2016) Noise Elimination Based on Moving Average by Guassian Distribution Weighting Method. Proceeding in 2nd International Conference on Control, Automation and Robotics (ICAAR). doi: 10.1109/ICCAR.2016.7486720

411 Fiorillo F (2011) Tank-reservoir drainage as a simulation of the recession limb of karst spring hydrographs, Hydrogeol J
412 19:1009–1019. doi:10.1007/s10040-011-0737-y

413 Fiorillo F, Doglioni A (2010) The relation between karst spring discharge and rainfall by cross-correlation analysis
414 (Campania, Southern Italy). Hydrogeol J 18(8):1881–1895. DOI 10.1007/s10040-010-0666-1

415 Fiorillo F, Pagnozzi M, Ventafridda G (2015a) A model to simulate recharge processes of Karst Massifs. Hydrol Process
416 29:2301–2314. doi:10.1002/hyp.10353

417 Fiorillo F, Petitta M, Preziosi E, Rusi S, Esposito S, Tallini M (2015b) Long term trend and fluctuations of karst spring
418 discharge in a Mediterranean area (central-southern Italy). Environ Earth Sci, 74:153–172. doi:10.1007/s12665-014-
419 3946-6

420 Fiorillo F, Pagnozzi M (2015) Recharge process of Matese karst massif (southern Italy). Environ Earth Sci 74:7557–
421 7570. DOI 10.1007/s12665-015-4678-y

422 Fiorillo F, Leone G, Pagnozzi M, Catani V, Testa G, Esposito L (2019) The upwelling groundwater flow in the karst area
423 of Grassano-Telese springs (Southern Italy). Water 11(5). doi:10.3390/w11050872

424 Fiorillo F, Leone G, Pagnozzi M, Esposito L (2021) Long-term trends in karst spring discharge and relation to climate
425 factors and changes. Hydrogeol J 29(1): 347–377. doi:10.1007/s10040-020-02265-0

426 Fleming SW, Lavenue AM, Aly AH, Adams A (2002). Practical applications of spectral analysis to hydrologic time
427 series. Hydrol Process 16:565-574. DOI: 10.1002/hyp.523

428 Ford D, Williams P (2007) Karst hydrogeology and geomorphology. Wiley, England.

429 Galli P, Giaccio B, Messina P, Peronace P, Amato V, Naso G, Nomade S, Pereira A, Piscitelli S, Bellanova J, Billi A,
430 Blamart D, Galderisi A, Giocoli A, Stabile T, Thil F (2017) Middle to Late Pleistocene activity of the northern Matese
431 fault system (southern Apennines, Italy). Tectonophysics 699:61–81. https://doi.org/10.1016/j.tecto.2017.01.007

432 Hyndman RJ, Athanasopoul G (2018) Forecasting: Principles and Practice. Monash University, Australia.

433 Kramer SL (1996) Geotechnical Earthquake Engineering. Prentice Hall, Upper Saddle River, New Jersey.

434 Larocque M, Mangin A, Razack M, Banton O (1998) Contribution of correlation and spectral analyses to the regional
435 study of a large karst aquifer (Charente, France). J Hydrol 205:217–231.

436 Leone G, Pagnozzi M, Catani V, Ventafridda G, Esposito L, Fiorillo F (2021) A hundred years of Caposele spring
437 discharge measurements: trends and statistics for understanding water resource availability under climate change. Stoch
438 Environ Res Risk Assess 35:345–370. https://doi.org/10.1007/s00477-020-01908-8

439 Leone G, Catani V, Pagnozzi M, Ginolfi M, Testa G, Esposito L, Fiorillo F (2022) Hydrological Features of Matese Karst
440 Massif, Focused on Endorheic Areas, Dolines and Hydroelectric Exploitation. Journal of Maps.
441 https://doi.org/10.1080/17445647.2022.2144497

442 Petrella E, Celico F (2009) Heterogeneous aquitard properties in sedimentary successions in the Apennine chain: case
443 studies in southern Italy. Hydrol Process 23:3365–3371. DOI: 10.1002/hyp.7441

444 Rufino F, Cuoco E, Busico G, Caliro S, Maletic EL, Avino R, Darrah TH, Tedesco D (2021). Deep carbon degassing in
445 the Matese massif chain (Southern Italy) inferred by geochemical and isotopic data. Environ Sci Pollut Res Int
446 28(34):46614–46626. doi:10.1007/s11356-020-11107-1

Silverii F, D'Agostino N, Borsa A, Calcaterra S, Gambino P, Giuliani R, Mattone M (2019) Transient crustal deformation from karst aquifers hydrology in the Apennines (Italy). Earth Planet Sci Lett 506:23–3. https://doi.org/10.1016/j.epsl.2018.10.019

Silverii F, D'Agostino N, Métois M, Fiorillo F, Ventafridda G (2016) Transient deformation of karst aquifers due to seasonal and multiyear groundwater variations observed by GPS in southern Apennines (Italy). J Geophys Res Solid Earth 121. doi:10.1002/2016JB013361

White AM, Gardner WP, Borsa AA, Argus DF, Martens HR (2022) A review of GNSS/GPS in hydrogeodesy: Hydrologic loading applications and their implications for water resource research. Water Resour Res 58(7). https://doi.org/10.1029/2022WR032078

White WB (2002) Karst hydrology: recent developments and open questions. Eng Geol 65:85–105.

458 **FIGURES**

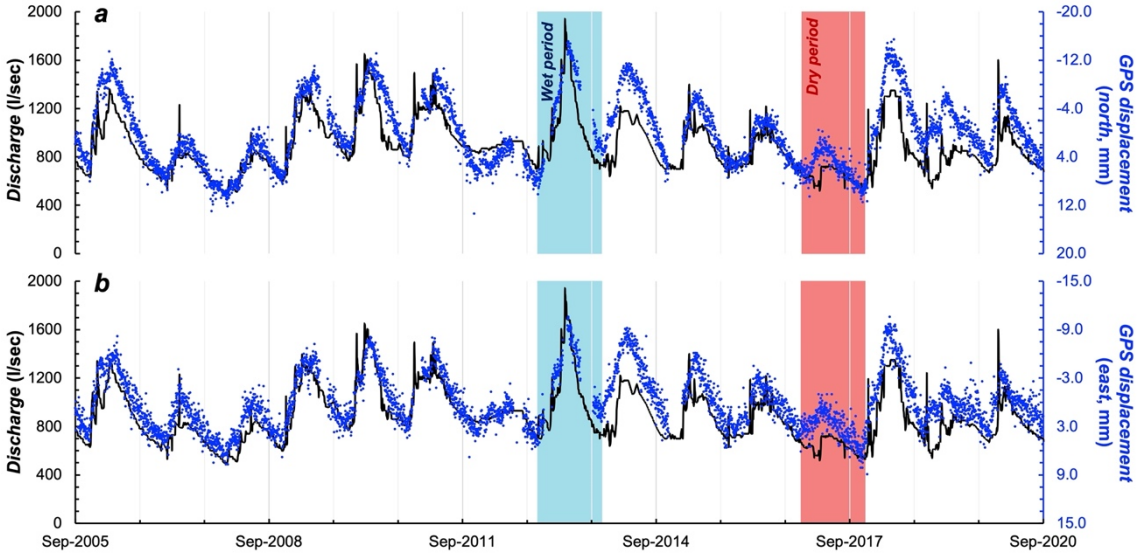

459

460 **Figure 1** Long-term time series of Maretto karst spring discharge (170 m a.s.l., Matese massif), black line, and horizontal
461 displacement of *VAGA* GPS station (736 m a.s.l.), blue dots (daily data). Colors highlight the wettest (2011-2012) the
462 driest (2016-2017) hydrological years of the time series.

463

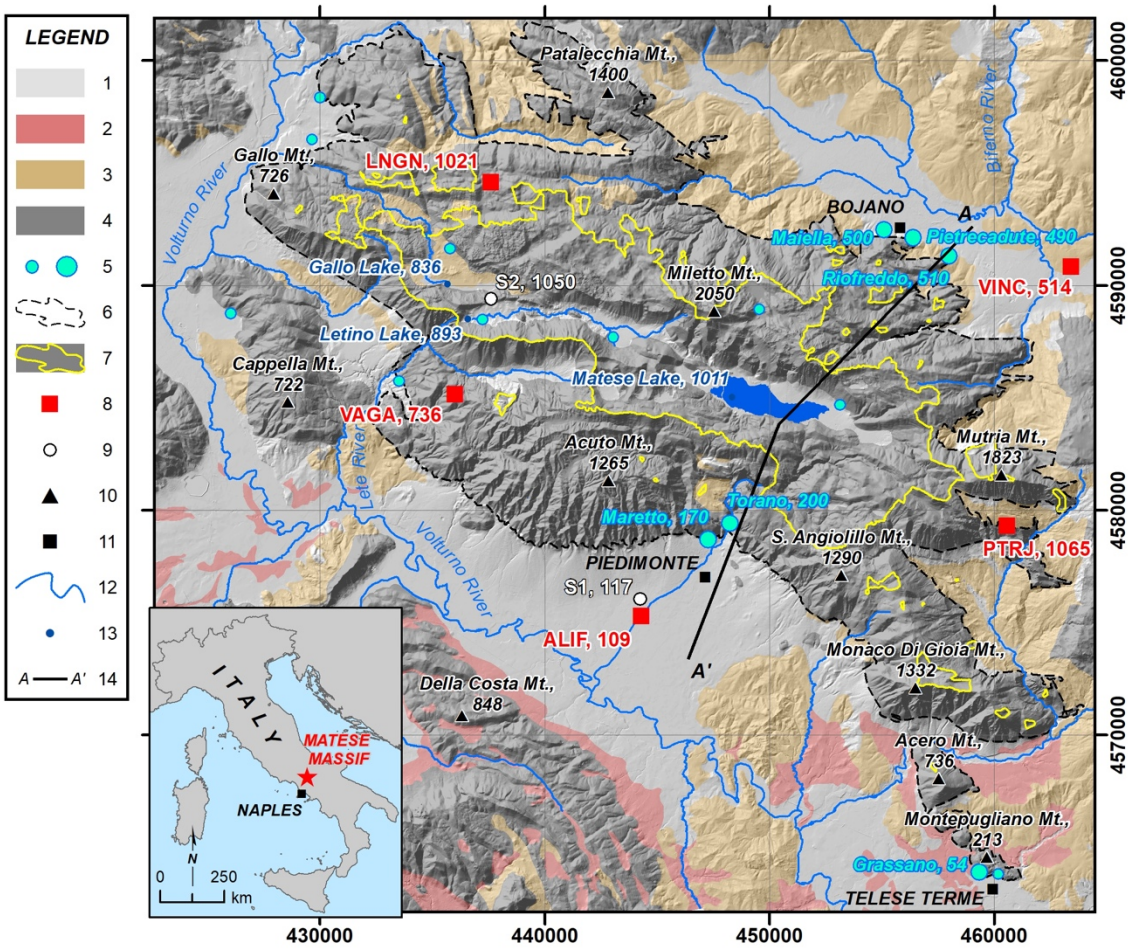

Figure 2 Geological sketch of the Matese karst area. Legend: 1) slope breccias and debris, alluvial, lacustrine and travertine deposits (*Quaternary*); 2) pyroclastic deposits (*Quaternary*); 3) argillaceous complexes and flysch sequences (*Paleogene-Miocene*); 4) dolomite-limestone sequences (*Jurassic-Miocene*); 5) main karst spring (small circle symbol) and major karst basal spring (big circle symbol, with elevation in m a.s.l.); 6) boundary of the Matese karst massif; 7) internal runoff area; 8) GPS station (with elevation); 9) meteorological station (with elevation); 10) mountain peak (with elevation); 11) main village; 12) major river; 13) lake elevation; 14) trace of the hydrogeological cross-section shown in Figure 8.

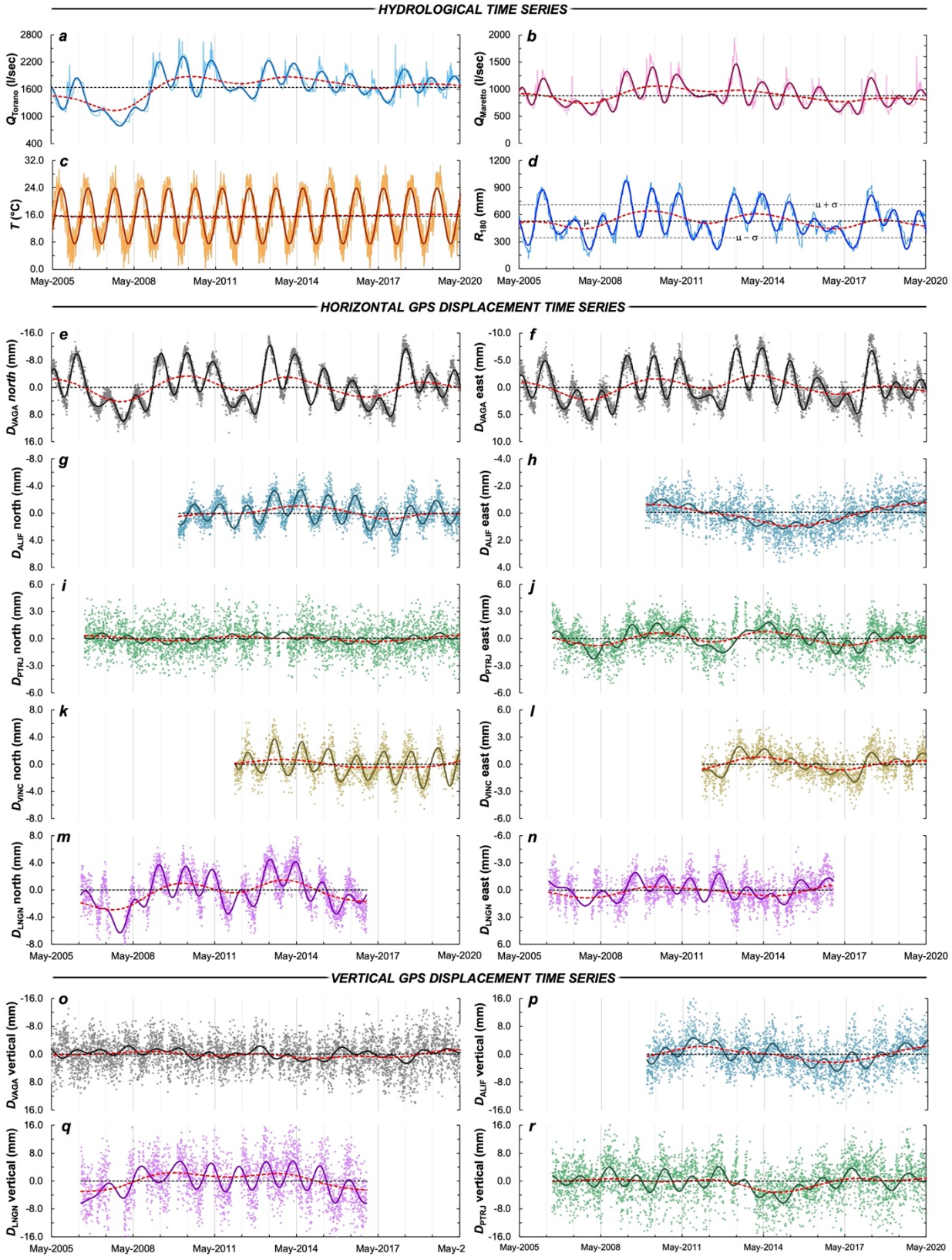

Figure 3 Hydrological time series of spring discharge (***a*** and ***b***), temperature (***c***), and 180-day cumulative rainfall (***d***), against horizontal displacement, *D*, north and east, time series for the different GPS stations (***e-n***). Note that the ordinate axis has been reversed in figures ***e-f***, ***g-h***, ***n*** and ***o***. Black dashed lines indicate the time series mean (□). Grey dashed lines in figure ***d*** indicate the mean plus and minus the standard deviation (σ). Smoothed colored curves were calculated by FFT-based analysis, while red dashed curves represent the 4-year Gaussian moving average.

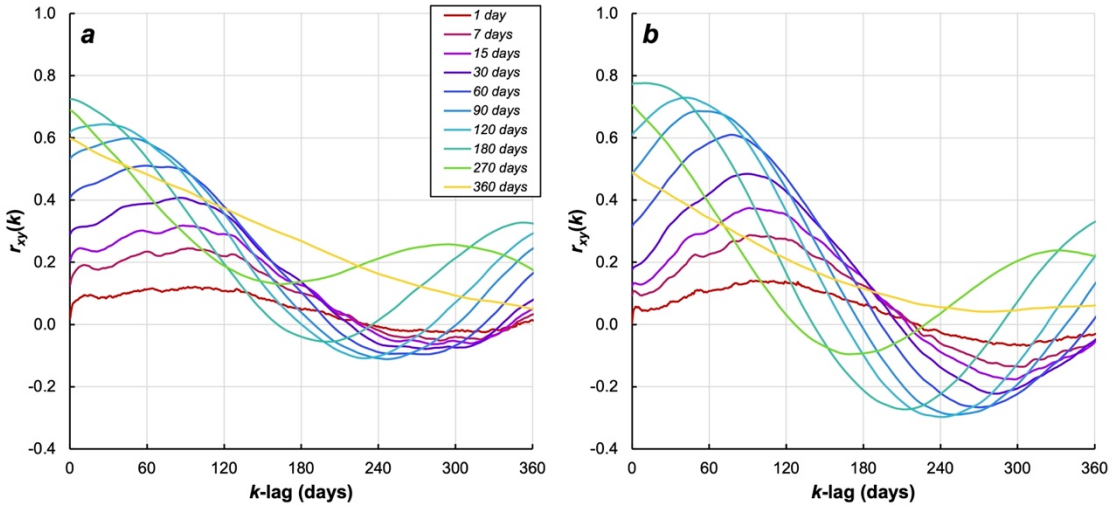

Figure 4 Cross-correlation functions between rainfall cumulated over period of different length (Alife rain gauge, *S1* station in **Figure 2**) and discharge of Torano (***a***) and Maretto (***b***) karst springs. Raw time series were used for cross-correlation analysis.

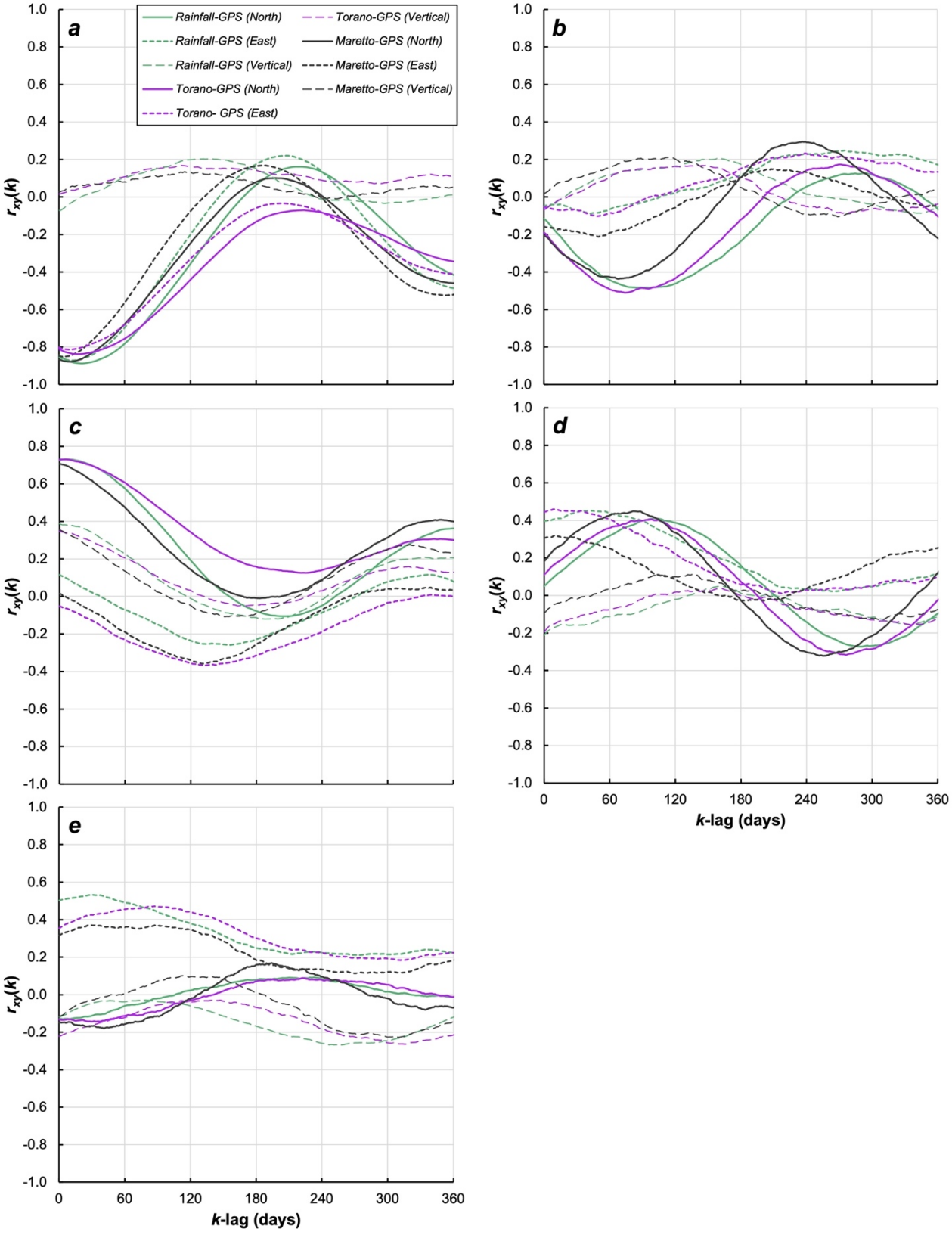

Figure 5 Cross-correlation between hydrological records (rainfall, and Torano and Maretto spring discharge; time series of *x*) and displacement data of five GPS stations (lagged time series of *y*): *VAGA* (***a***), *ALIF* (***b***), *LNGN* (***c***), *VINC* (***d***), *PTRJ* (***e***). Note that time series of 6-month rainfall was used for panels from ***a*** to ***d***, and 9-month rainfall for panel ***e***. Raw time series were used for cross-correlation analysis.

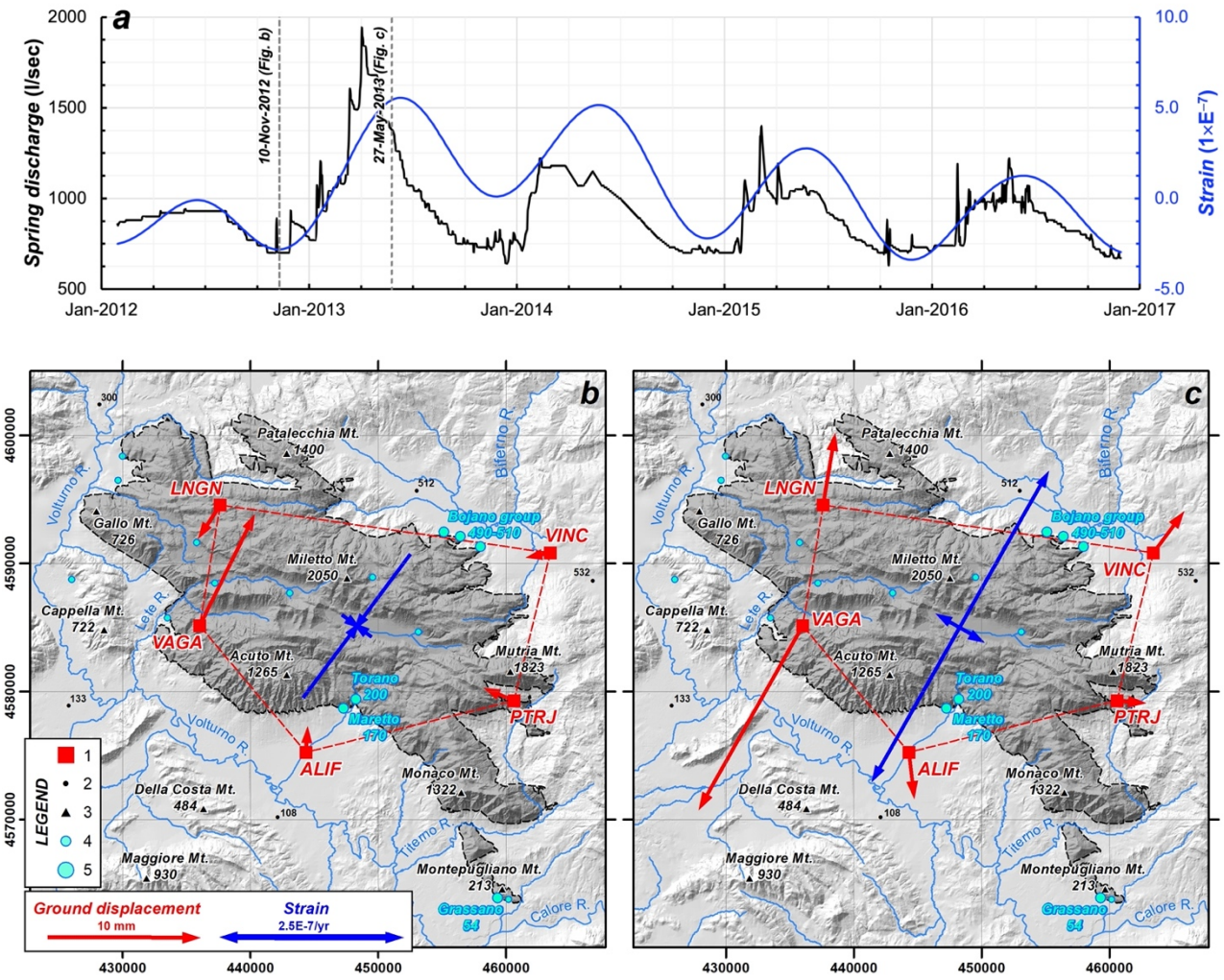

Figure 6 (***a***) Time series of Maretto karst spring and temporal evolution of the horizontal estimated strain ($\varepsilon_{xx} + \varepsilon_{yy}$) in the polygon joining stations in the Matese massif (red dashed line in panels ***b*** and ***c***), highlighting the strong correlation between horizontal deformation and hydraulic conditions in the Matese aquifer; positive strain values indicate dilatation, while negative values indicate contraction. GPS displacements (red arrows) and strain estimated (blue diverging and converging arrows) for 2 snapshots representative of high (***b***) and low spring discharge conditions (***c***; see the Supplementary Material for the continuous evolution). The Matese karst massif was emphasized with a grayish tone.

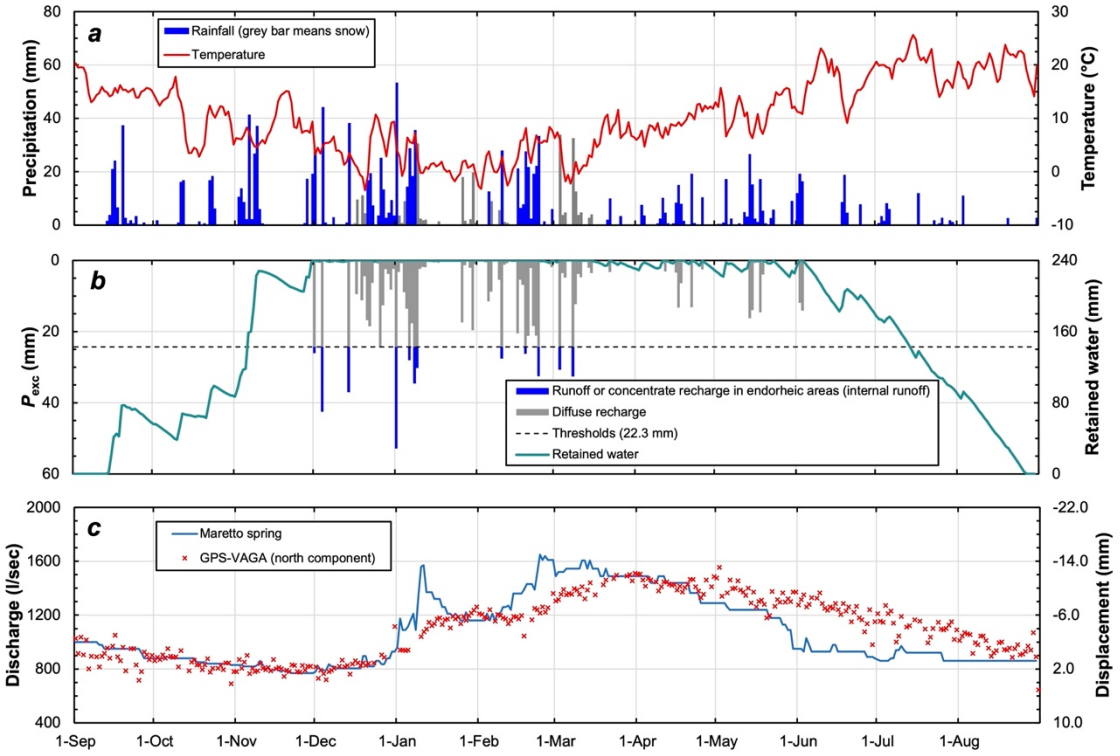

Figure 7 Daily recharge model applied for the 2009-2010 hydrological year. Panel ***a*** shows rainfall, snow, and temperature records of Letino climate station (*S2*), located at 1050 m a.s.l. in western sector of the Matese massif. Panel ***b*** illustrates the simulated precipitation excess, P_{exc}, which was split into recharge and runoff (or concentrate recharge in endorheic areas) by a rainfall threshold value of 24.3 mm; simulated retained water was also shown, which was obtained from soil hydrological balance. Panel ***c*** shows discharge of Maretto spring and observed GPS displacement of *VAGA* station (north component).

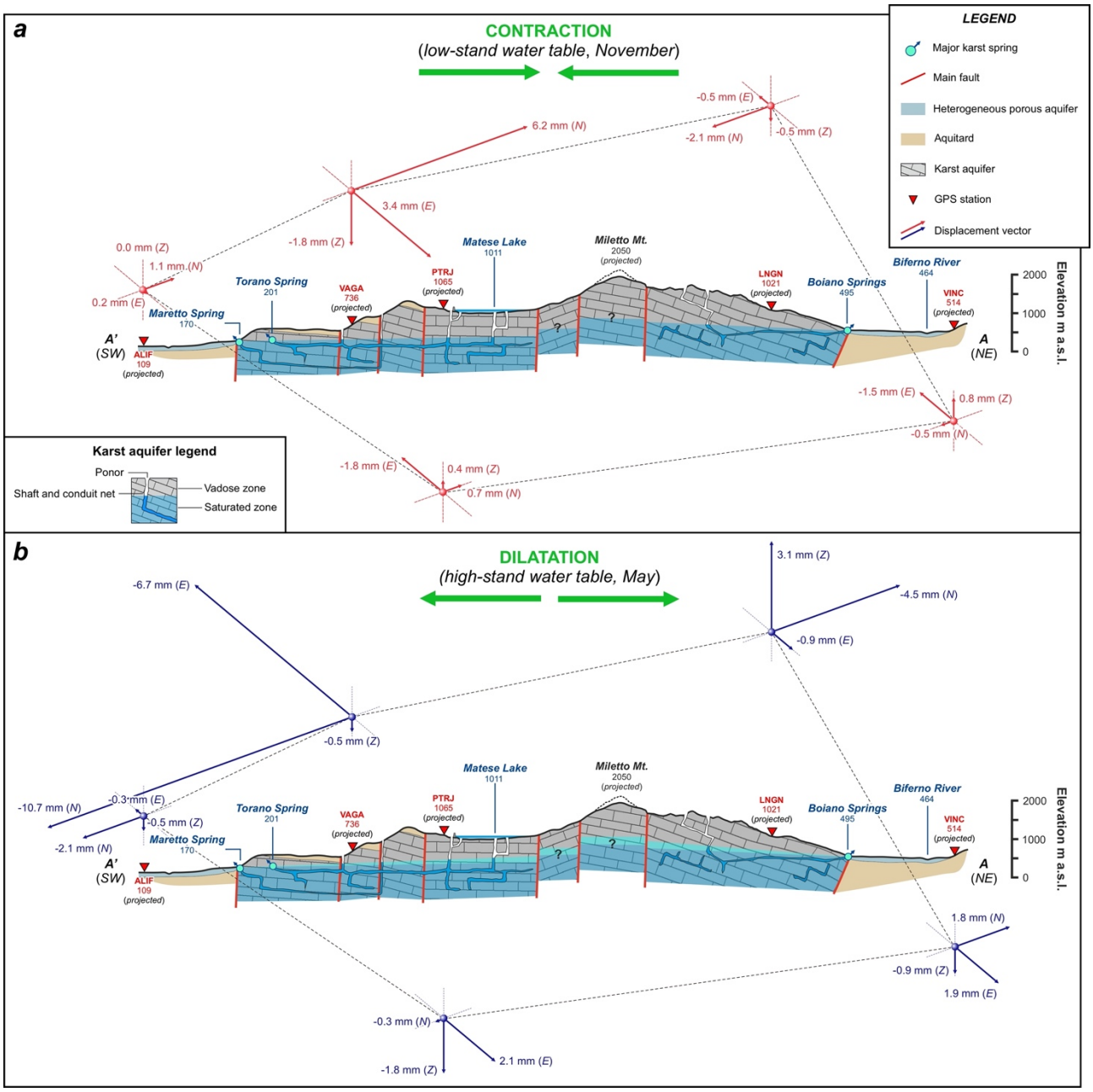

Figure 8 Hydrogeological sketch of the Matese karst massif (modified from Fiorillo and Pagnozzi 2015; section trace is shown in **Figure 2**) illustrating two different stage of the water table height (November 2012 and May 2013). Groundwater conditions in dry season (low flow; ***a***) and wet season (high flow, ***b***) are shown, along with components of the vertical (*Z*) and horizontal displacements (*N* and *E*) recorded by GPS stations.